Program Digest, 2019 IEEE International Ultrasonics Symposium (IUS)
Glasgow, Scotland, October 6-9, 2019

Minimally Invasive InVivo Functional Ultrasound Imaging Using a 40 MHz Phased Array Endoscope: Mapping the Auditory Response in Rats

Christopher Samson
Biomedical Engineering
Dalhousie University
Halifax, Canada
samsonchris.cs@gmail.com

Thomas Landry
Department of Surgery
Nova Scotia Health Authority
Halifax, Canada
tglandry@dal.ca

Jeremy A. Brown
Biomedical Engineering, Electrical and Computer Engineering
Dalhousie University
Halifax, Canada
j.brown@dal.ca

***Abstract*— Recently, functional ultrasound imaging has emerged as a new tool for monitoring changes in cerebral blood volume associated with neural activity. The combination of high spatiotemporal resolution as well as low cost and high portability have positioned ultrasound to potentially become a ground-breaking imaging modality for functional imaging of the brain. To date, studies have been limited to large craniotomies, neonatal, and thin skull applications. In this study we extend the application of functional ultrasound to small burr hole surgeries by using a 64-element 40 MHz phased array packaged in a 2.5 × 3.1 mm endoscopic form factor. In anesthetized rats, the probe was inserted into a small 3.0 × 6.5 mm hole for functional imaging of the inferior colliculus (IC) which is an important node in the auditory neural pathway. 4, 8, and 15 kHz tones were presented at 97 dB for fixed intervals. Imaging was undertaken during these intervals by coherently compounding 16 diverging waves at a pulse repetition frequency of 40 kHz on a custom 64-channel beamforming platform. Image acquisition and stimulus were synchronized and automated using a custom Python 2.7 software interface. Beamforming, singular-value decomposition (SVD) filtering, and post-processing were performed in MATLAB. Increases in cerebral blood volume as high as 85% were measured in response to auditory stimuli in the IC. Mapping was performed with very high spatial resolution, 40 and 100 µm of axial and lateral resolution respectively. The position of the measured functional activation is in excellent agreement with the anatomical position of the IC. This study shows that functional mapping through small burr hole surgeries is possible, vastly increasing the number of potential use-cases for functional ultrasound imaging.**

Keywords—Functional ultrasound, high-frequency ultrasound imaging, ultrafast imaging

I. Introduction

The emergence of ultrafast beamforming strategies based on coherent compounding has dramatically improved Doppler capabilities for ultrasound imaging. Exploiting the high temporal resolution of ultrafast ultrasound techniques such as plane and diverging wave imaging has improved the signal-to-noise ratio and sensitivity of Doppler measurements, and has lead to the development of functional ultrasound imaging. By closely monitoring the power Doppler signal, changes in cerebral blood volume can be used as a surrogate for neural activity [1]–[8]. The combination of high spatiotemporal resolution of ultrasound imaging, as well as the low cost and portability of ultrasound imaging systems relative to more commonly used functional imaging modalities such as functional magnetic imaging (fMRI), and positron emission tomography (PET), position functional ultrasound as a potentially ground-breaking tool for both preclinical and clinical applications.

For neurosurgical applications, intraoperative functional mapping of the brain is critical for preserving healthy brain tissue. The use of electrocortical stimulation mapping (ESM), is the primary intraoperative mapping tool used by neurosurgeons. Clinical data suggests that it improves successful tumor resection rates from 58.1% without ESM mapping to 74.9% of cases when ESM is issued prior to resection [9], [10]. Functional mapping is therefore of paramount importance in improving a neurosurgeon's confidence in segmenting healthy tissue from tumors. Despite being the gold standard for functional mapping, ESM presents a risk of inducing seizures [11], [12] and is limited to topical mapping. Previous work by Imbault et al. has shown that functional ultrasound is capable of functional cortical mapping, matching the results of ESM in both the motor and somatosensory cortices in humans [1]. Therefore, functional ultrasound provides surgeons with similar surface-level mapping as ESM but adds depth-resolved functional information not previously available to clinicians. The clinical potential of this technology to improve surgical outcomes is evident. The study undertaken by Imbault et al. was performed with a large craniotomy, allowing for the topical application of a large linear array [1]. Despite the impressive potential of this technology, many neurosurgeries are performed through small burr-holes which do not allow the topical application of large linear arrays.

In this work, a 64-element 40 MHz phased array [13] with an endoscopic form factor of 2.5 × 3.1mm is leveraged to dramatically reduce the minimum allowable craniotomy size so that functional ultrasound can be used as a guidance tool. The endoscopic probe was inserted inside a 3.0 × 6.5 mm craniotomy

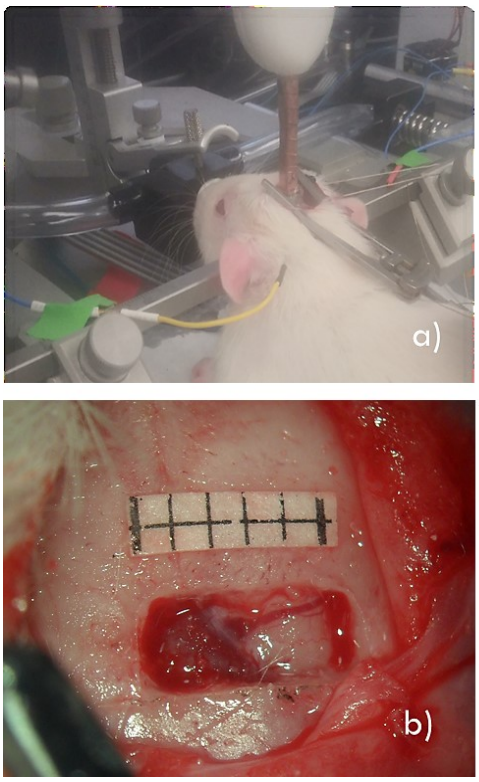

Fig 1. (a) Surgical craniotomy with endoscopic probe inserted. The rat's head is securely positioned using metal ear bars and a vaporizer that delivers isoflurane. Electrodes are inserted into the skin for ABR measurements. (b) A close-up view of the craniotomy with a 2 x 5 mm grid reference.

of an anaesthetized rat, exposing the inferior colliculus (IC) under ultrasound guidance. Functional mapping of auditory neural activation was successfully measured in the IC with the application of auditory stimuli at various tones.

II. Methods

A. Imaging

Imaging was performed using a 64-element 40 MHz phased array. The array is tightly packaged into a 2.5 × 3.1 mm form factor manufactured in accordance with [13] and provides roughly 40 and 100 µm of axial and lateral resolution respectively. The imaging window ranges from 3 to 10 mm depths at viewing angles ranging from ±32°. Given a 1λ element-to-element pitch, this relatively narrow field of view is used to mitigate grating lobe artifacts. Beamforming is performed on a custom 64-channel high-frequency beamforming platform capable of storing 64 transmit insonifications of channel data in hardware before transferring the data to a PC through a USB 3.0 interface [14]. The system pulse repetition frequency is 40 kHz. Each frame is beamformed by coherently compounding 16 diverging waves whereby 49 elements are active for each diverging wave, and the angular aperture for each diverging is set to 90°, in accordance with the diverging wave beamforming strategy outlined in [15]. Each insonification is performed with a 3-cycle pulse, and the full aperture is used to receive with no apodization.

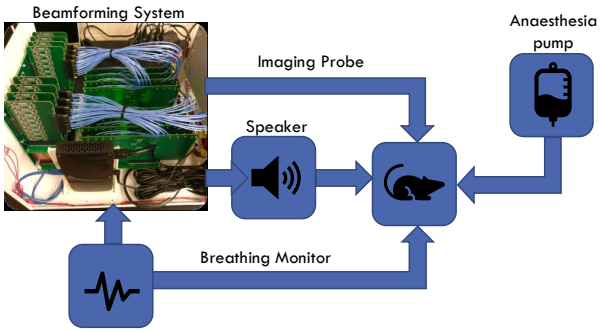

Fig 2. Experimental setup for mapping auditory responses to stimuli using functional ultrasound.

B. Animal Preparation

The experimental procedures were approved by the Dalhousie University Committee on Laboratory Animals. The rats were anesthetized using isoflurane during the investigation. A small craniotomy, 3.5 × 6 mm, was drilled through each rat's skull, exposing the brain. Hollow metal ear bars were inserted into the ear canals, serving both the purpose of positioning the rat into a stereotactic positioning stage and to provide a controlled pathway for closed auditory stimulation. An auditory brainstem response (ABR) test was then performed, ensuring that each rat's hearing was normal and auditory stimuli were being effectively delivered before conducting a functional ultrasound investigation. Fig 1 a) shows the surgical preparation, and Fig 1 b) highlights the particularly small size of the craniotomy by placing a 2 x 5 mm reference grid in the field of view.

C. Experimental Setup

With the animal situated under anesthesia, the imaging probe was mounted using a stereotactic 3-axis mechanical translation stage. A tweeter speaker (Tymphany XT25TG30-04, San Rafael, California) was connected to the left metal ear bar using rubber tubing. The sound intensity is held constant across the frequencies and is delivered to the ear canal via the ear bars (4, 8, and 15 kHz). The speaker was driven using a function generator with continuous-wave tones (Tektronics AFG3101C, Beaverton, Oregon) at intensities calibrated to give 97 dB SPL at each tone frequency. The function generator was

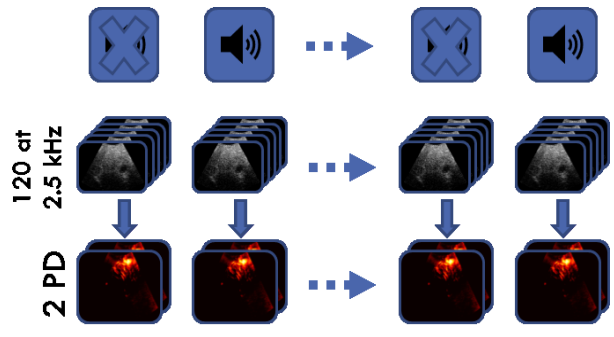

Fig 3. Functional ultrasound imaging sequencing. Baseline and stimulus power Doppler images are acquired alternatively. Each acquisition yields 2 power Doppler images derived from 120 B-mode images captured at 2.5 kHz.

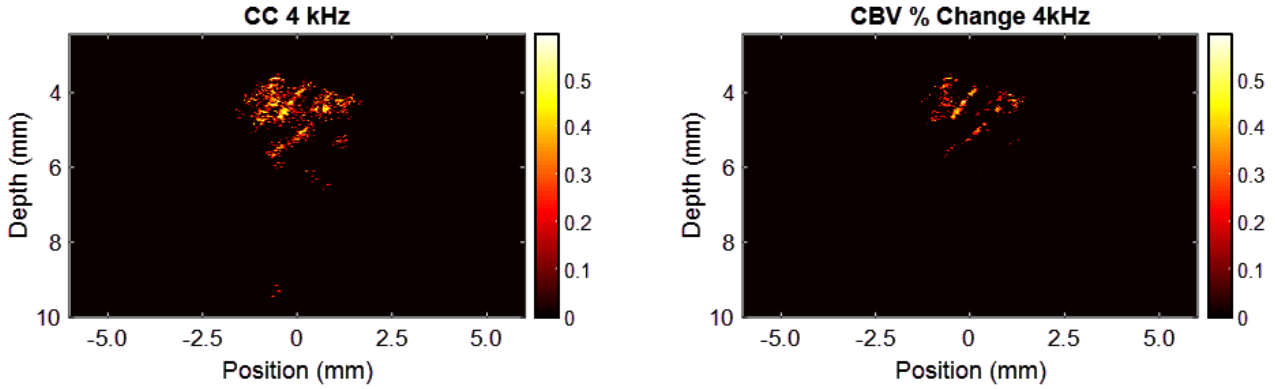

Fig 4. Functional activation in response to a 97 dB 4 kHz tone. (a) shows the Pearson correlation coefficient mapping with a threshold of r = 0.26 (p-value = 0.05). (b) % change in CBV processed with a simple spatial filter.

turned on and off by a custom Python 2.7 software interface that synchronized auditory stimulus with an ultrafast imaging sequence. Imaging was also gated by the rat's breathing cycle which was monitored using a piezoelectric bimorph placed under its chest. Under flexion, the bimorph outputs an analog signal which was used to trigger an oscilloscope (Keysight MSO-X 2024A, Santa Rosa, California), which provided an external trigger to a second function generator (Tektronics AFG3101C, Beaverton, Oregon), which provided a level-shifted acquisition gating signal to the beamforming system. This reduced motion artifacts that would otherwise be introduced by pulmonary inhalation and exhalation. Fig 3 provides a visualization of the experimental configuration.

D. Functional Ultrasound Imaging

Baseline measurements were acquired for 2 s followed by 2 s of acquisitions with auditory stimulus applied. These measurements were repeated across 10 iterations for each tone. Fig 3 shows the sequence of events where 120 B-mode images are captured in succession for each 2 s window. An ensemble of 60 B-mode images was used for each power Doppler frame. The peak imaging rate was 2.5 kHz for 16 diverging waves. Channel data for 60 frames were transferred to the PC every second. All beamforming and signal processing was performed in MATLAB (Mathworks, Natick, Massachusetts). A singular value decomposition filter was applied to the B-mode frames to separate the blood signal from the brain parenchyma [16].

III. Experimental Results and Discussion

Functional activation was successfully recorded in the IC using a minimally invasive craniotomy. Fig 4 a) shows the Pearson correlation coefficient mapping of the IC using a threshold at r = 0.26 (p-value = 0.05). The functional activation was anatomically confined to the IC, with no neighboring tissue showing signs of functional activation. In Fig 4 b) the changes in cerebral blood volume in response to a 4 kHz tone are shown. Changes in blood volume greater than 20% are shown, as the system is only capable of reliably discerning changes in blood volume exceeding this threshold. The peak changes detected in this study were 85% before spatial filtering was applied and plotted as is shown in Fig 4 b).

Fig 5 (a)-(c) overlays the functional activation in response to 4, 8, and 15 kHz tones on top of high-quality B-mode images. The spatial resolution of the functional mapping is remarkable, with roughly 40 and 100 µm of axial and lateral resolution respectively. Fig 5 shows correlations greater than r = 0.26 (overlaid onto B-Mode images where 4, 8 and 15 kHz tone functional maps are shown respectively). The position of functional activation is in excellent agreement with the anatomical position of the IC which walls between 3 to 6 mm from the surface of the rat brain. The strongest activation was recorded at 4 kHz, with reduced activation intensity at 8 and 15 kHz.

The data collection for this study was done at much slower rates than conventional methods due to the bottleneck of

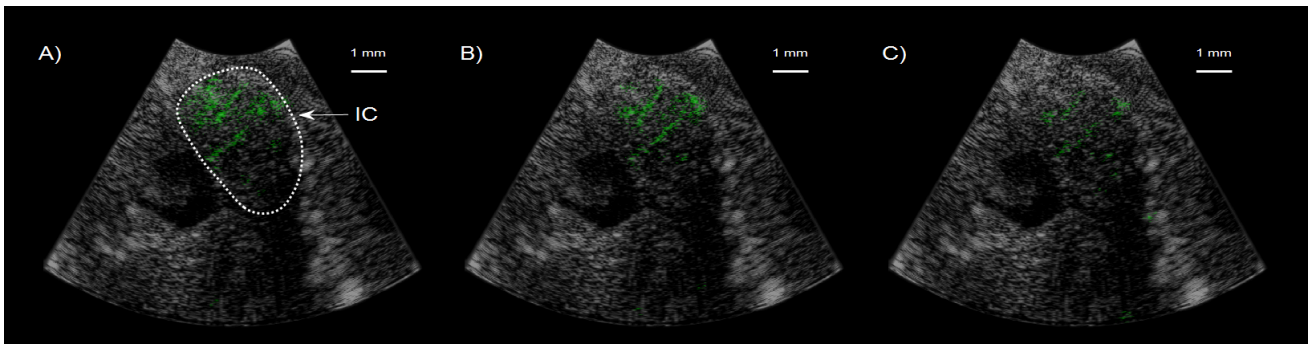

Fig 5. Functional activation in response to auditory stimuli is overlaid onto B-mode images. Activation is localized in the IC with parts (a)-(c) showing the change in activation in response to 4, 8, and 15 kHz tone respectively.

transferring data from the beamforming platform to the PC. As such, there was a significant gap between groups of B-mode images used to process the power Doppler frames. Since the system can acquire and store 64 insonifications worth of channel data, 4 frames can be generated from 16 diverging waves at an effective frame rate of 2.5 kHz. However, data transfer to the PC limits the acquisition rate of successive groups of 4 frames since all data needs to be transferred to the PC before collecting 64 subsequent insonification, or 4 new B-mode frames compounded from 16 diverging waves. This limited the acquisition to 60 B-mode frames per second, but amazingly, functional data was still extractable, mostly due to the powerful suppression of the parenchyma from the SVD filter. In future work, hardware-based beamforming will be utilized to dramatically improve the system frame rate by reducing the data transfer bottleneck and adding onboard storage for hundreds of ultrafast B-mode frames. This improvement is likely to dramatically improve system SNR and sensitivity to small changes in cerebral blood volume.

Despite this data transfer limitation, this pilot study shows the potential for functional mapping through minimally invasive craniotomies. Functional activation was detected at depth and the endoscopic nature of this imaging probe would allow neurosurgeons to push the endoscope down brain sulci for improved image guidance and functional mapping. As further experiments are conducted, the confidence level of the thresholding is also expected to increase, reflecting the natural increases in SNR and sensitivity expected with improved beamforming hardware.

IV. Conclusion

This study shows that functional mapping through small burr hole surgeries is possible, vastly increasing the number of potential use-cases for functional ultrasound imaging. Functional mapping of the auditory response in the inferior colliculus was successfully performed using 4, 8, and 15 kHz tones. This technology has the potential for reducing post-operative neurological deficits by providing functional mapping that would otherwise not be possible in burr hole surgeries using state-of-the-art ESM mapping, especially in cases where ESM mapping within the sulci is not possible.

References

[1] M. Imbault, D. Chauvet, J.-L. Gennisson, L. Capelle, and M. Tanter, “Intraoperative functional ultrasound imaging of human brain activity,” *Scientific reports*, vol. 7, no. 1, p. 7304, 2017.

[2] E. Macé, G. Montaldo, I. Cohen, M. Baulac, M. Fink, and M. Tanter, “Functional ultrasound imaging of the brain,” *Nature methods*, vol. 8, no. 8, p. 662, 2011.

[3] T. Deffieux, C. Demene, M. Pernot, and M. Tanter, “Functional ultrasound neuroimaging: a review of the preclinical and clinical state of the art,” *Current opinion in neurobiology*, vol. 50, pp. 128–135, 2018.

[4] É. Macé, G. Montaldo, S. Trenholm, C. Cowan, A. Brignall, A. Urban, and B. Roska, “Whole-brain functional ultrasound imaging reveals brain modules for visuomotor integration,” *Neuron*, vol. 100, no. 5, pp. 1241–1251, 2018.

[5] B.-F. Osmanski, C. Martin, G. Montaldo, P. Lanièce, F. Pain, M. Tanter, and H. Gurden, “Functional ultrasound imaging reveals different odor-evoked patterns of vascular activity in the main olfactory bulb and the anterior piriform cortex,” *Neuroimage*, vol. 95, pp. 176–184, 2014.

[6] C. Bimbard, C. Demene, C. Girard, S. Radtke-Schuller, S. Shamma, M. Tanter, and Y. Boubenec, “Multi-scale mapping along the auditory hierarchy using high-resolution functional UltraSound in the awake ferret,” *Elife*, vol. 7, p. e35028, 2018.

[7] E. Mace, G. Montaldo, B.-F. Osmanski, I. Cohen, M. Fink, and M. Tanter, “Functional ultrasound imaging of the brain: theory and basic principles,” *IEEE transactions on ultrasonics, ferroelectrics, and frequency control*, vol. 60, no. 3, pp. 492–506, 2013.

[8] M. Gesnik, K. Blaize, T. Deffieux, J.-L. Gennisson, J.-A. Sahel, M. Fink, S. Picaud, and M. Tanter, “3D functional ultrasound imaging of the cerebral visual system in rodents,” *NeuroImage*, vol. 149, pp. 267–274, 2017.

[9] P. D. W. Hamer, S. G. Robles, A. H. Zwinderman, H. Duffau, and M. S. Berger, “Impact of intraoperative stimulation brain mapping on glioma surgery outcome: a meta-analysis,” *J Clin Oncol*, vol. 30, no. 20, pp. 2559–2565, 2012.

[10] H. Duffau, M. Lopes, F. Arthuis, A. Bitar, J. Sichez, R. Van Effenterre, and L. Capelle, “Contribution of intraoperative electrical stimulations in surgery of low grade gliomas: a comparative study between two series without (1985-96) and with (1996-2003) functional mapping in the same institution,” *Journal of Neurology, Neurosurgery \& Psychiatry*, vol. 76, no. 6, pp. 845–851, 2005.

[11] F. Roser and M. Liebsch, “Closer to the Edge-The Value of Intraoperative Brain Mapping.,” *World neurosurgery*, vol. 89, pp. 689–691, 2016.

[12] S. Ille, N. Sollmann, T. Hauck, S. Maurer, N. Tanigawa, T. Obermueller, C. Negwer, D. Droese, C. Zimmer, B. Meyer, and others, “Combined noninvasive language mapping by navigated transcranial magnetic stimulation and functional MRI and its comparison with direct cortical stimulation,” *Journal of neurosurgery*, vol. 123, no. 1, pp. 212–225, 2015.

[13] A. Bezanson, R. Adamson, and J. Brown, “Fabrication and performance of a miniaturized 64-element high-frequency endoscopic phased array.,” *IEEE Trans Ultrason Ferroelectr Freq Control*, vol. 61, no. 1, pp. 33–43, 2014.

[14] C. A. Samson, A. Bezanson, and J. A. Brown, “A sub-nyquist, variable sampling, high-frequency phased array beamformer,” *IEEE transactions on ultrasonics, ferroelectrics, and frequency control*, vol. 64, no. 3, pp. 568–576, 2016.

[15] C. Papadacci, M. Pernot, M. Couade, M. Fink, and M. Tanter, “High-contrast ultrafast imaging of the heart,” *IEEE transactions on ultrasonics, ferroelectrics, and frequency control*, vol. 61, no. 2, pp. 288–301, 2014.

[16] C. Demené, T. Deffieux, M. Pernot, B.-F. Osmanski, V. Biran, J.-L. Gennisson, L.-A. Sieu, A. Bergel, S. Franqui, J.-M. Correas, and others, “Spatiotemporal clutter filtering of ultrafast ultrasound data highly increases Doppler and fUltrasound sensitivity,” *IEEE transactions on medical imaging*, vol. 34, no. 11, pp. 2271–2285, 2015.